Proc. Int. Conf. Neutron Optics (NOP2017)
JPS Conf. Proc. **22**, 011019 (2018)
https://doi.org/10.7566/JPSCP.22.011019

Recent Developments SoNDe High-Flux Detector Project

Sebastian Jaksch[1], Ralf Engels[2], Günter Kemmerling[2], Uwe Clemens[3], Sylvain Désert[4], Hanno Perrey[5,6], Codin Gheorghe[7], Arne Fredriksen[7], Petter Øya[7], Henrich Frielinghaus[1], Kevin Fissum[6], Amanda Jalgén[6], Emil Rofors[6], Kalliopi Kanaki[5], Richard Hall-Wilton[5,8], Ramsey al Jebali[5]

[1]*FZ Jülich GmbH, Jülich Centre for Neutron Science JCNS at Heinz Maier-Leibnitz Zentrum, D-85747 Garching, Germany*
[2]*FZ Jülich GmbH, Jülich Centre for Neutron Science JCNS, D-52428 Jülich, Germany*
[3]*FZ Jülich GmbH, Zentralinstitut für Engineering, Elektronik und Analytik (ZEA-2), D-52428 Jülich, Germany*
[4]*LLB, CEA, CNRS, Universtité Paris-Saclay, CEA Saclay, F-91191 Gif-sur-Yvette, France*
[5]*European Spallation Source ESS ERIC, P.O. Box 176, SE-221 00 Lund, Sweden*
[6]*Division of Nuclear Physics, Lund University, SE-221 00 Lund, Sweden*
[7]*Integrated Detector Electronics AS IDEAS, NO-0484 Oslo, Norway*
[8]*Mid-Sweden University, SE-851 70 Sundsvall, Sweden*

E-mail: s.jaksch@fz-juelich.de

(Received September 6, 2017)

New high-flux and high-brilliance neutron sources demand a higher count-rate capability in neutron detectors. In order to achieve that goal, the Solid-State Neutron Detector (SoNDe) project is developing a scintillation-based neutron detector. It will be capable of fully exploiting the available flux at small-angle neutron scattering (SANS) instruments at high brilliance sources, such as SKADI at the European Spallation Source (ESS). The read-out of the scintillator is based on a pixelized multi-anode PMT (MaPMT), where each pixel is treated separately. In addition to enabling higher achievable count-rates, one of the design goals was to develop a modular and scalable solution that can also be used in other instruments or even contexts, such as for laboratory setups. This has been achieved by combining the complete read-out electronics along with the MaPMT into modules that can be controlled and read-out individually via a network without additional any infrastructure. An overview of the present state of development and current test results is presented, highlighting the results of previously published project reports.

KEYWORDS: detector, neutron, scintillation, scintillator, SANS, reflectometer, neutron instrumentation, neutron detector

1. Introduction

The development of ever brighter and more brilliant neutron sources [1, 2] calls for a concurrent development in detector technology to be able to fully exploit the better sources to capacity. Along high rate capability, other key parameters include position resolution, detection efficiency, low sensitivity to backgrounds, time resolution, ease of use, reliability and maintainability and the accessibility of necessary materials. The detector technology discussed here is based on the requirements of the SANS instrument SKADI [3] to be constructed at the ESS.

In order to address these issues, the SoNDe detector technology has been developed based upon the following design criteria:

- count-rate capability of at least 20 MHz over a 1×1 m^2 detector area, quadrupling the rate capabilities of existing technologies [4]

- Pixel resolution of 3×3 mm^2, and even better by using Anger interpolation
- Neutron-detection efficiency higher than 80% with good γ-discrimination
- ^{3}He independence
- μs time resolution
- Consisting of individual modules, that can operate independently

Achieving these capabilities simultaneously will allow a high-performance neutron detector. Apart from the ability to use this detector in large-scale facilities where count-rate capability is the principal concern, the other design criteria allow for use in different fields, e.g. bench-top laboratory experiments or even mobile applications, such as scanning for fissionable material in shipped goods [5]. Additional background information on the tests described here can be found in the previously published project reports [5].

2. Basic Concept

The basic concept of the SoNDe design is the pixelization of the detector area, both to distribute a high local count-rate over several analogue channels as well as to increase the resulting spatial resolution. This is coupled with the idea of having black-box electronics for the read-out located directly behind the MaPMT to facilitate the read-out. Such a setup facilitates upscaling when larger areas are to be equipped with modules next to each other, which also leads to the requirement, that the electronics be no larger than the preceeding MaPMT in order to allow for a close packaging and therefore avoid dead space between the individual modules. A sketch of the dense packing is shown in Fig. 1.

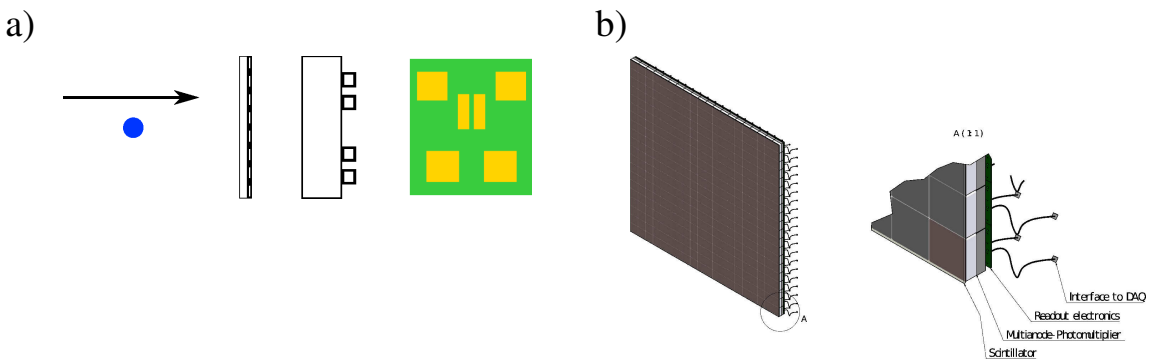

Fig. 1. a) Sketch of the basic concept of a SoNDe detector module. The neutrons (blue) are coming from the left hand side and then impinge on the scintillation material, which is pixelized in this case. The following MaPMT converts the scintillation light into an electronic signal, which is then processed by the read-out electronics. As shown here, all components have an identical footprint, facilitating dense packaging. b) Possible large-scale arrangements

Specific challenges to this design include the prevention of cross-talk between the pixels, which here is inhibited by grooving the scintillator, as well as the packing density of the electronics behind the MaPMT.

As stated earlier, such a setup can be used to create larger surface area detectors as shown in Fig.1 b). It is important that the single modules can be packed as closely as possible. This packaging simultaneously fulfills the requirement of ease of maintenance, as each single module can be serviced individually, while the large-scale setup is not impacted in any major way. This allows also arrangements with different geometries that can be used to improve the performance of neutron-scattering

instruments. One such example might be the arrangement of the modules on a surface of a sphere to cover the entire scattering solid angle without any detector movement.

In the following sections, scintillation material, MaPMT and electronics are discussed individually. A performance overview for the modules will then be presented.

2.1 Components of the detector modules

2.1.1 Scintillator

The scintillator used for the SoNDe modules is a ^{6}Li GS20 glass scintillator purchased from Scintacor®. A general description of such scintillators can be found in Refs. [6–9]. A 6.6% ^{6}Li content leads to a thermal neutron efficiency of ≈75% in a 1 mm thick sample, higher for cold neutrons. With the current setup each neutron-event results in approximately 6600 scintillation photons with a peak wavelength of 390 nm . Approximately 10% of the scintillation light reaches the photocatode corresponding to a MaPMT pixel. The decay time of the light emission is about 60 ns, which does not impede the overall dead-time in our setup. [5].

The γ-sensitivity of GS20 Li-glass is strongly dependent on the γ-energy. For γ-energies of less than 1 MeV, the γ-detection can be suppressed by pulse-height discrimination. Higher γ-energies, suppression is an issue, as these γ cannot be distinguished from neutrons using pulse height discrimination.

In order to assess the cross-talk between pixels we investigated possibilities for a physical separation between the pixels of the scintillator. A method for doing so is attaching the scintillator glass onto a carrier glass and then grooving the scintillator glass with a wafer saw. By doing so, the cross-talk was reduced drastically (see Fig.2). Note that channels 0-7 and 55-63 are at the top and bottom of the MaPMT, which results in a slightly different gain values. Hence, the cross-talk in those channels deviates from the overall average. It also should be noted that the contributions of the other components to the cross-talk, such as the MaPMT and potential electronic cross-talk, are always contained in the results given. Since we only varied the scintillator, these other contributions can be considered to be constant and are not relevant for an optimization of the scintillator.Finally we note that the carrier glass may improve the light yield per pixel by total internal reflection [5].

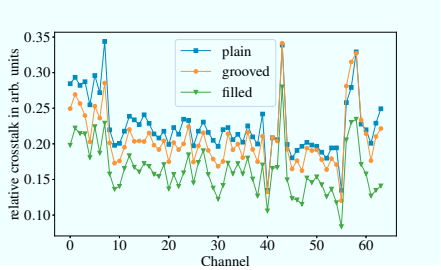

Fig. 2. Relative cross-talk between the MaPMT pixels for a plain scintillator, a grooved scintillator with 200 μm wide grooves and the same grooves filled with reflecting correction fluid. In both cases, the grooves penetrated the entire scintillator (1 mm). The cross-talk is normalized to the amount of neighbours per pixel.

2.1.2 Multi-anode Photomultiplier

The MaPMT used for these detector modules is the Hamamatsu H8500 with 64 channels, each 6×6 mm^2, and a total active area of 52×52 mm^2. The later H12700 series MaPMTs are also technically compatible, as well as the H9500 and their successors with a 3×3 mm^2 pixel size [10]. MaPMTs are vacuum tubes containing a photosensitive cathode and several dynode stages, where multiplication of the initial charge occurs. The choice of these devices over silicon based photomultipliers

(SiPMs) was deliberate, in order to avoid radiation damage by doping the silicon with neutrons. The electronics behind the MaPMT seem to be protected from neutron radiation by the boron in the front glass [5, 11]. While the detailed tests in the manuscript focus on the H8500 MaPMTs, the others were only examined in preliminary tests.

2.1.3 Read-out electronics

In order to confine the read-out electronics to the preceding scintillator and MaPMT, they are logically divided into a front-end board and a controller board. The front-end board houses the ASICS used for reading out the MaPMT channels directly. The controller board houses the FPGA module, power supply and an Ethernet port for communication with the back-end computer. A block diagram is shown in Fig.3. This is a direct representation of the schematic given in Fig.1 a).

Depending on the setting, either the analogue event energy or a trigger signal indicating a detected event can be forwarded to the controller board. There, appropriate data treatment (time stamping, channel allocation) is performed and the data are then fed to the Ethernet interface. The module itself can be reached via its own IP address and is thus directly controllable. Programming of the FPGA for further logic operations and the inclusion of external data into the data stream is also possible.

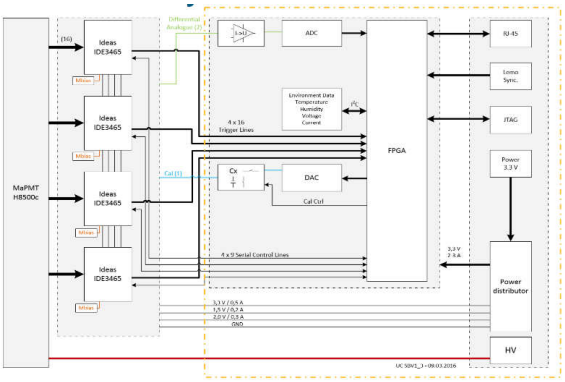

Fig. 3. Schematic diagram of the circuits in the SoNDe detector module. From left to right: The scintillation photons are converted into a current in the MaPMT, which is then registered by the 16 channel ASIC Ideas IDE3465. Here four of them are shown to support a 64 channel photomultiplier.

This setup has the advantage that each single module can be addressed using a computer via standard protocols (TCP and UDP). Therefore, no additional hardware is needed to operate the module, aside from a power source and a HV source for the MaPMT. Operations such as sensitivity calibrations and error messaging can be done online, either with an array of modules connected to a network or with a module directly attached to a PC.

3. Assembled Array

A 3D CAD model and a photograph of a fully assembled SoNDe module are shown in Fig.4. Apart from the Ethernet connection and a power supply for the modules and the MaPMT, there is no additional infrastructure necessary to read out incoming data from the modules. The different settings for the different function modes can be programmed using the PC software. The modules fully support the Ethernet standard and the TCP/UDP protocol and conventional network hardware can be used to connect.

a) b)

Fig. 4. a) Schematic of a fully assembled SoNDe module. The Trenz module (proprietary FPGA module) containing the FPGA (green), the controller board with ETHERNET, JTAG, LEMO and power connectors (blue) and the front-end board, housing the ASICs (yellow) can all be seen. Between the controller and the front-end board there is an aluminum heat sink, which also protects the bonding wires of the ASICs. The HV cable (red) is channeled past the PCBs. b) Photograph of four fully assembled modules configured in a 2×2 detector array. Edgeless packing allows the construction of large scale detectors with a tiled array.

4. Performance

In this section, the performance of the SoNDe detector modules is presented.

4.1 Initial Module

The first module was based on the IDEAS ROSMAP system [5]. Tests at the Laboratoire Léon Brillouin (LLB) were performed. Both the basic feasibility and the radiation hardness of the prototype were in the focus of the investigation.

As a full white beam was available at the beam line G3.2 [12], the flux capabilities of the module could be tested. In order to do so, a fully absorbing slit system was positioned in front of the module and the beam size was increased until the response became non-linear. The corresponding data is shown in Fig.5. The count-rate increases linearly with the irradiated area until 250 kHz, which is the

a) b)

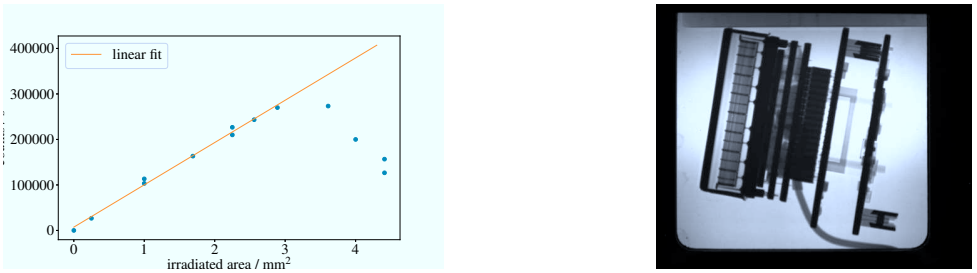

Fig. 5. a) Relation between irradiated area and count-rate. b) Radiograph of the first generation SoNDe Module. It is visible that the boron glass at the front of the MaPMT is nearly intransparent to neutrons. With an additional scintillator in front of the module, the combined shielding effect of the scintillator and the boron glass effectively protect the electronics from radiation damage.

rate-limit for this module. At higher count-rates, double counting below the dead-times occurs. 250 kHz on a single $52 \times 52\,\mathrm{mm}^2$ module correspond to 100 MHz on a full square meter detector. Here, it has to be taken into account that the signal was simply detected and that no data treatment inside the module was performed. Also, for a clear separation between each neutron-event, a buffer-time

between events is usually inserted into the logic of the modules. This was omitted here and trigger settings could only be adjusted manually by increasing the threshold until a sufficient background suppression was reached. Thus, this has to be seen as the maximum achievable count-rate with that setup. This is also illustrated by the fact that the physical dead-time of the scintillator (60 ns) corresponds to a maximum possible count-rate of 16.67 MHz in the same location, which here is alleviated by using a non infinitesimally small surface area, however the hard physical limit is nearly in the same order of magnitude.

In order to test the radiation hardness the module was kept in continuous operation under the maximum achievable neutron flux for 10 days, during that time only one single event upset occurred after nine days. A restart and subsequent electronic test showed that no permanent damage was inflicted upon the module. The module electronics, seem to be inherently stable under high radiation conditions. This is likely due to the fact that direct exposure to the neutron beam is blocked by both the scintillator itself and the subsequent boron glass in the MaPMT. We estimate that between them, they attenuate the neutron flux to less than 1% of its initial value. This effect can also be seen in the radiography image of the module shown in Fig. 5.

4.2 Second-Generation SoNDe module

The second generation module was described in detail in Ref. [5]. The test was performed at the TREFF instrument at Heinz Maier-Leibnitz Zentrum (MLZ), Garching, at a neutron wavelength of 4.7 Å. During these tests, both the performance under actual experimental conditions as well as the status of the software were tested. While the electronics were demonstrated to handle high count-rates with a pulse generator on the benchtop, it was important to make sure that this was also true for statistically distributed pulses generated by the MaPMT. The control software, which will be needed for the ongoing testing, was also tested.

The test beam was tailored by two blinds to yield a vertical stripe of neutrons on the detector. This was done to make sure that in the non-irradiated areas no event could be triggered. This could lead to background in later application of the module. An image of the detected neutron-events on the demonstrator surface is shown in Fig.6. There is no visible saturation. The recorded pulse-height spectrum allows for a clear discrimination between neutron and γ-events.

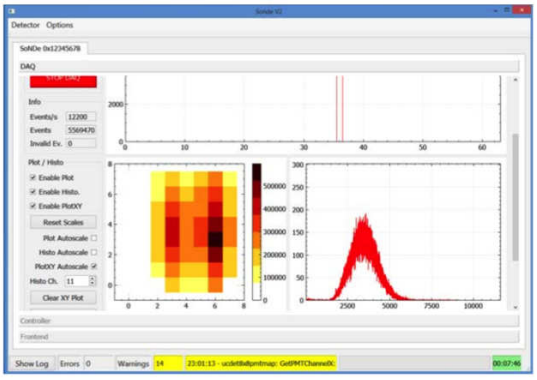

Fig. 6. Screenshot of the SoNDe control software during operation.

All information was visualized and recorded using the control software (screenshot Fig.6). There, distribution of the events across the face of the MaPMT as a function of pixel together with the corresponding pulse-height spectrum is shown. Additionally, each submodule of the 2×2 demonstrator can be accessed via a separate register card. Only one submodule was connected. These tests showed

that the performance of the 2×2 demonstrator under actual experimental conditions achieved the expectations. The integrated flux in the primary beam of the TREFF instrument is $\approx 10^8$ neutrons/s and no saturation effects of any kind are visible. Confirmation of these results by future tests on higher flux instruments is foreseen. The development of SoNDe can now proceed to the upscaling to larger areas.

4.3 Electronic performance

The second-generation SoNDe module was tested with a pulse generator. Dynamic range, maximum count-rate and single-event detection were evaluated [5]. The dynamic range was determined by examining the linearity of the relationship between input charge and ADC signal. The results are shown in Fig.7 a). Between 9.4 and 80 pC, the ADC signal was completely linear as a function of the integrated input charge. Saturation effects become visible above 80 pC, a dynamic range of about one order of magnitude. This linearity allows for a reliable discrimination of the signal.

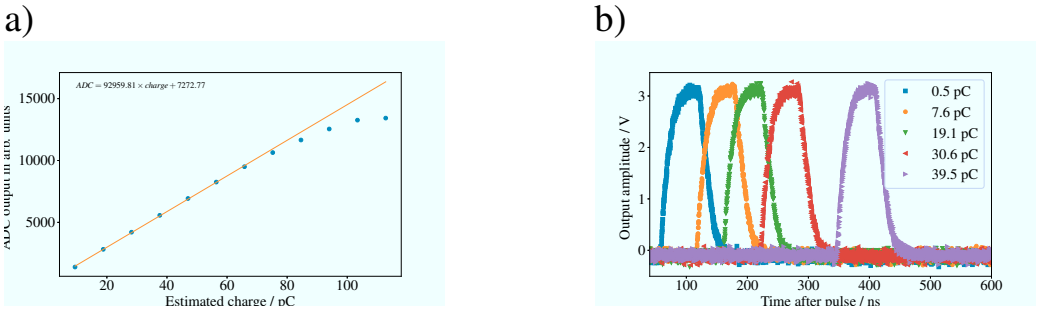

Fig. 7. a) Relationship between integrated input charge and ADC value. b) Time delay between the initial pulse at the input of the module and the resulting digital trigger signal. The time delay varies depending on the pulse charge and the threshold setting.

In order to assess the maximum achievable count-rate, the system was fed with an increasing frequency of pulses from the generator until a loss was observed. While the system exhibited stable behaviour up to 2.22 MHz, at 2.23 MHz some pulses were lost. In the case of statistical pulses, a counting frequency of about 10% is assumed, hence translating the maximum frequency into ≈ 220 kHz for stable operation. Achieving this for a 1 m^2 detector area would translate into 400×220 kHz= 88 MHz as the maximum stable event rate.

Finally, an evaluation of single events revealed that the processing delay through the front-end board was 110 ns for each detected event, completely independent of the irradiated pixel. The charge required to trigger the system rises along with the trigger threshold. The time to trigger the system increases with the threshold. The corresponding behaviour of the trigger signals can be seen in Fig.7. Lower thresholds lead to a faster detection of the signal. This is expected as lower input charges need to be integrated over longer times in order to exceed a given threshold value. Both the fixed delay and the relation between threshold and event charge have to be taken into account for the later time stamping of events. The accuracy of the time stamp delivered by the module is approximately ±150ns.

5. Conclusion

We have presented an overview of the present state of the SoNDe detector technology. The results show that the construction of a high-flux neutron detector with 6×6 mm^2 resolution is possible. An upgrade path to 3×3 mm^2 resolution has already been identified as feasible. Maximum obtainable

count-rates could exceed 20 MHz per square meter. In terms of maintenance and operation, both the radiation hardness of the single modules as well as their ease of operation has been established. The modular design facilitates any repair and maintenance work in later assemblies.

Acknowledgments

The work on the SoNDe project is funded by the European Union within the Horizon 2020 framework under project number 654124. The financial support by the European Union is gratefully acknowledged. We also gratefully acknowledge beam-time both at Laboratoire Léon Brillouin (LLB) and Heinz Maier-Leibnitz Zentrum (MLZ).

References

[1] S. Peggs, R. Kreier, C. Carlile, R. Miyamoto, A. Påhlsson, M. Trojer, J. G. Weisend, *et al.*, eds., *ESS technical design report*. European Spallation Source, 2013.

[2] O. Kirstein, R. Hall-Wilton, I. Stefanescu, M. Etxegarai, M. Anastasopoulos, K. Fissum, A. Gulyachkina, C. Höglund, M. Imam, K. Kanaki, *et al.*, "Neutron position sensitive detectors for the ess," *arXiv preprint arXiv:1411.6194*, 2014.

[3] S. Jaksch, D. Martin-Rodriguez, A. Ostermann, J. Jestin, S. D. Pinto, W. Bouwman, J. Uher, R. Engels, and H. Frielinghaus, "Concept for a time-of-flight small angle neutron scattering instrument at the european spallation source," *Nuclear Instruments and Methods in Physics Research Section A: Accelerators, Spectrometers, Detectors and Associated Equipment*, vol. 762, pp. 22–30, 2014.

[4] A. Radulescu, N. K. Szekely, and M.-S. Appavou, "Kws-2: Small angle scattering diffractometer," *Journal of large-scale research facilities JLSRF*, vol. 1, p. 29, 2015.

[5] S. Jaksch, R. Engels, G. Kemmerling, C. Gheorghe, P. Pahlsson, S. Désert, and F. Ott, "Cumulative reports of the sonde project july 2017," *arXiv preprint arXiv:1707.08679*, 2017.

[6] F. Firk, G. Slaughter, and R. Ginther, "An improved li6-loaded glass scintillator for neutron detection," *Nuclear Instruments and Methods*, vol. 13, pp. 313–316, 1961.

[7] A. Spowart, "Neutron scintillating glasses: Part 1: Activation by external charged particles and thermal neutrons," *Nuclear Instruments and Methods*, vol. 135, no. 3, pp. 441–453, 1976.

[8] A. Spowart, "Neutron scintillating glasses: Part ii: The effects of temperature on pulse height and conductivity," *Nuclear Instruments and Methods*, vol. 140, no. 1, pp. 19–28, 1977.

[9] E. Fairley and A. Spowart, "Neutron scintillating glasses part iii pulse decay time measurements at room temperature," *Nuclear Instruments and Methods*, vol. 150, no. 2, pp. 159–163, 1978.

[10] . H. P. K.K, "Flat panel type multianode pmt assembly h8500 series / h10966 series," 2011.

[11] M. Andreotti, W. Baldini, R. Calabrese, G. Cibinetto, A. C. Ramusino, C. Dedonato, M. Fiorini, E. Luppi, R. Malaguti, A. Montanari, *et al.*, "Radiation damage effects in silicon photo-multipliers," in *Nuclear Science Symposium and Medical Imaging Conference (NSS/MIC), 2013 IEEE*, pp. 1–4, IEEE, 2013.

[12] A. Menelle, "www-llb.cea.fr/fr-en/pdf/description-g3bis-g32-g5bis-v3.pdf," tech. rep., CEA Saclay, 2011.